![frontiers] **Frontiers in Physics**

Check for updates

Hall currents and EDL effects on multiphase wavy flow of Carreau fluid in a microchannel having oscillating walls: A numerical study

M. M. Alqarni[1†], Arshad Riaz[2*†], Muazma Firdous[3†],
Ikram Ullah Lali[4†], ElSayed M. Tag El-Din[5†] and
Shafiq ur Rahman[3†]

[1]Department of Mathematics, College of Sciences, King Khalid University, Abha, Saudi Arabia, [2]Department of Mathematics, Division of Science and Technology, University of Education, Lahore, Pakistan, [3]Department of Computer Science, University of Chakwal, Chakwal, Pakistan, [4]Department of Information Sciences, Division of Science and Technology, University of Education, Lahore, Pakistan, [5]Faculty of Engineering and Technology, Future University in Egypt, New Cairo, Egypt

In this analysis, the authors reveal the effects of electro-osmosis on the multiphase flow of Carreau fluid in a microchannel in the presence of Hall currents and solid particles. Moreover, the compliant channel walls are subject to oscilluation occurring at the surface. To investigate the problem quantitatively, mathematical models for fluid phase and particulate phase have been structured. A lubrication approach is adopted due to laminar flow and the small dimensions of the channel. To produce the data, a system of differential equations is produced with the help of a numerical process performed on Mathematica through a built-in NDSolve tool. The results are presented graphically to examine the effects of various physical factors on the flow quantities. From pictorial discussion, it is gathered that the Helmholtz−Smoluchowski velocity parameter and the presence of an increasing amount of solid particles increasing the heat exchange while producing electro-kinetic energy. It is also found that velocity is a direct function of solid particles and compliant walls, but an inverse link is seen in the presence of electro-kinetic energy. Such studies can be employed with microfluidic devices and \may also be productive in medical and mechanical research.

KEYWORDS

Carreau fluid, elastic compliant walls, hall currents, electro-osmois, multiphase flow, numerical results

Introduction

For a long time, many scientists have considered peristaltic transport in fluid mechanics to identify its importance in medical fields (in general) and hydrodynamics (in particular). A pumping flow is created by waves spread along the adaptable channel walls. This procedure encounters numerous organic frameworks involving transportation using plane muscles, e.g., the motion of food along the intestinal tract, the transportation of urine, the course of blood in the capillaries, and so on. This subject has received extensive analysis (for various liquids and various channels). The peristaltic transport system attracted additional interest following the examination performed by Latham [1]. Then, Fung and Yih [2] added a commitment to the major investigation of the peristaltic scheme by utilizing the fixed flow frame exhibited by Shapiro et al. [3] in moving frame transformations. Following that, a few examinations were performed to measure the way that peristalsis of different liquids behaves, using lubrication technology (see Refs. [4–8]).

Studies containing two-phase flow due to newly added solid fragments in a base liquid using a variety of conduits has been conducted by many researchers. The hypothetical investigation of these frameworks is vital in actual peculiarities, such as fluidization, lunar debris streams, paint splashes, atomic reactor cooling, and disintegration. The uses of such streams can be seen in medication and geoscience. The hypothesis of particulate-fluid mixture has been used to examine organic streams like those of blood [9, 10]. Recently, the concatenation of an induction of particles in fluids has been identified by numerous researchers. Bhatti et al. [11] explored the issue of a pumping stream with wall slip. This stream was incited by a sinusoidal wave. They likewise examined the endoscopic impacts on the dual phase solution. Srivastava and Srivastava [12] analyzed the peristaltic scheme of rheological fluid utilizing a Casson stress matrix. In a further review, they utilized a particulate-fluid suspension streaming in a body with a pumping procedure [13]. Misra and Pandey [14] developed a particle-fluid flow study in a round and hollow cylinder, in which the stream is produced by a progressive wave. Yamane et al. [15] dealt with the consistent advancement of a particulate solution in a rotating pipe. Later, Bhatti et al. [16] utilized a blood coagulation structure to observe the intensity of motion in a dusty fluid considering a changeable thickness for a wavy movement of fluid. Akbar et al. [17] introduced a numerical model prompted by a ciliary movement within the sight of a magnetic field with a copper type of nano particles. Rashed and Ahmed [18] recently published a work on the peristaltic flow of a dusty liquid concentration of nanofluid across a bended enclosure and produced the reading that large Eckert numbers introduce increased heat and speed of fluid and dusty phases.

Most commonly used liquids are non-Newtonian in their behavior. From raw petroleum unsheathing to the materials business, from thermoplastic industry to medication, and

from the assembly of different lubricants to biological blood streams, we intensely rely upon the various types of non-Newtonian liquids. Different numerical tensors for non-linear liquids have been presented by specialists, with reference to the physical and warm qualities of these liquids. Akbar and Nadeem [19] worked on the creeping movement of the Jeffrey stress model by considering a variable viscosity model and heat exchange phenomenon. In this study, it is found that the Jeffrey fluid model imposes an opposite impact on amount of pressure increase, but the heat transfer rate is enhanced in case of variable viscosity attributes. Nazeer et al. [20] investigated two phase flows of non-Newtonian fluid in a heated, inclined conduit, having compliant walls and permeable medium. A lubrication approximation is taken into account to achieve the final form of the flow model exhibiting the physical face of the study. The results of that work have been constructed as follows: the permeability of the free space exerts an inverse impact on temperature of the fluid, and due to radiation effects, the velocity is declines. Saleem et al. [21] described an electro-osmotic analysis for a multiphase flow of a Jeffrey stress model. Tiny spherical particles are considered in the base fluid, and the exact results are framed. The conclusion suggests that electro-kinetic energy can be suitably increased by providing the amount of zeta potential. Riaz and Sadiq [22] published a solid particulate-liquid suspension of the Eyring–Powell expression through a curved channel. The problem is managed with the application of linearity and smoothness constraints. Perturbation technology is adopted to evaluate the analytical data and the result is produced that the presence of solid particles decreases the fluid's speed as well as its pressure profile. The most common practically used fluid model is the Carreau fluid model, but in the literature, work with this model is rare due to its complicated mathematical stress expression. This model is very useful for its dual characteristics, in that it behaves as a Newtonian at low shear rates and as a non-Newtonian fluid for the median rate of applied stress. Noreen et al. [23] investigated heat exchange analysis in pumping the transport of Carreau fluid flowing in an inclined geometry and suggested that this model be linked to a blood flow in capillary and microvessels. It is claimed that stream boluses are less dragged for Carreau fluid than viscous fluid. Recently, Asha and Belery [24] solved the problem of the peristaltic pumping of Carreau fluid in the presence of Joule's heating by employing a multi-step DTM, and their results showed that the Grashof number reduces the velocity in half of the channel and increases in the other half, while temperature distribution is enhanced by heat absorption factor and the Brickman number. Further work on Carreau fluid can be found in [25–28].

Electroosmotic studies have been seen to a significant degree for many years. The principal gadget-like Microelectromechanical System (MEMS) was the microfluidic innovation collected during the 1980s. Such devices can be applied across a range of contexts containing natural and

physiological sectors, where microfluidic items are termed LOCs (lab-on-chip devices). LOC devices can be utilized equally well for various targets, including physical therapeutics and microbial or toxic contamination. Currently, an there is a recognized need for minimal, straightforward, and cheap homogenized hardware for drug dispersal and DNA-based investigation in light of the requirement for viable, quick, and appreciable standardized quality of microfluidics. Devices are often used that drive liquid all through an entire network utilizing electroosmosis. Electroosmosis addresses the electrolyte stream across a channel with an external voltage unit limit. In a few organic, clinical, and producing systems, electroosmosis creates, including the dialysis of liquids, porous layers, zoological cycles, movement in human skin, a tube/waterway stream, and methods of separation. Yasmeen and Iqbal [29] presented electrical double layer (EDL) effects on the heat and mass convection analysis of a viscous fluid in a porous medium with consideration of peristaltic pumping. The authors found that the electro-osmosis factor can help reduce the permeability of the medium. In the work of Tripathi et al. [30], the unsteady flow of a viscous fluid is established through electro-osmosis and peristalsis. In this article, the authors find that electric potential is an inverse function of EDL, and the strong electric field puts an inverse impact on wall stress. Prakash and Tripathy [31] incorporated the EDL mechanism for a Phan–Thien–Tanner fluid in an asymmetric peristaltic enclosure using Poisson–Boltzman expression and established that the fluid flow is extensively affected by EDL thickness and electric field strength. Further work on electro-osmosis can be found in [32, 33].

Examination of the literature finds no study on the peristaltic mechanism of Carreau model multiphase flow with Hall currents and electroosmotic pumping. The rheological effects of the non-Newtonian (Carreau) and electro-kinetic properties of EDL make the problem more applicable in various clinical and mechanical fields. The current analysis focuses the numerical study of heat transfer in pumping flow of particulate-liquid (Carreau fluid) in the presence of EDL effects and Hall currents in a compliant channel. The equations are modeled using suitably applied lubrication theory and scaling transformations of a non-dimensionlization procedure. The achieved non-linear coupled differential equations are handled by a numerical approach using an in-house command of Mathematica. The results are elaborated pictorially by sketching the curves of velocity and temperature profiles against various factors. Moreover, the current analysis is compared with the results in the literature to establish the validity of the findings.

Mathematical structure

Let us assume an unsteady particulate-fluid transport of non-linear Carreau fluid containing tiny solid particles of non-variable density in a two-dimensional micro peristaltic

channel. An external battery is attached to the fluid phase container to produce electro-kinetic energy in the fluid phase. For simplicity, we neglect the effects of electro-osmosis on a particulate phase and a thermal profile. The walls of the conduit are taken to be oscillating at the surfaces. Geometrically, the waves are propagating along a horizontal axis $(\tilde{x})$ with a small uniform amplitude, and the flexible walls are taken as a function of vertical coordinate $\tilde{y}$ and time $\tilde{t}$, as disclosed in Figure 1.

A constant extrinsic magnetic strength B_0 is applied orthogonally on the flow direction. The mathematical representation of the wavy walls is delivered as [34]:

$$\pm H\left(\tilde{x}, \tilde{t}\right) = \pm\tilde{a} \pm \tilde{b} \sin\frac{2\pi}{\lambda}\left(\tilde{x} - \tilde{c}\tilde{t}\right), \qquad (1)$$

where $\tilde{a}$ is the channel's semi width, $\tilde{c}$ is the wave propagation speed, $\tilde{b}$ is the wave's average amplitude, $\tilde{t}$ is the time factor, and λ provides the wavelength.

The fluid phase with velocity decomposition as $V_f = (\tilde{u}_f, \tilde{v}_f)$ is presented as follows [20–28]:

$$\boldsymbol{\nabla} \cdot \boldsymbol{V}_f = 0, \qquad (2)$$

$$(1-C)\rho_f\left(\frac{\partial}{\partial\tilde{t}} + \boldsymbol{V}_f \cdot \boldsymbol{\nabla}\right)\boldsymbol{V}_f = -(1-C)\boldsymbol{\nabla}\tilde{P} + (1-C)\boldsymbol{\nabla}\cdot\boldsymbol{\tau}_f$$
$$- CS\left(\boldsymbol{V}_f - \boldsymbol{V}_p\right) + \boldsymbol{J}\times\boldsymbol{B} - \rho_e\boldsymbol{E}, \qquad (3)$$

$$(1-C)\rho_f c_P\left(\frac{\partial}{\partial\tilde{t}} + \boldsymbol{V}_f \cdot \boldsymbol{\nabla}\right)\tilde{T}_f = (1-C)\left(\boldsymbol{\tau}_f \cdot \boldsymbol{L}\right) + \frac{\rho_p c_P C}{\bar{\omega}_T}$$

$$\left(\tilde{T}_P - \tilde{T}_f\right) + k'(1-C)\boldsymbol{\nabla}^2\tilde{T}_f + CS\left(\boldsymbol{V}_f - \boldsymbol{V}_p\right)^2. \qquad (4)$$

The aforementioned relation contains the velocity vector V_f, the stress tensor for Carreau model $\boldsymbol{\tau}_f$, ρ_f the fluid's density, $\boldsymbol{J}\times\boldsymbol{B}$ the Lorentz force, $\boldsymbol{E}$ the electric field, c_p the specific heat, $\tilde{T}_f$ the temperature distribution, k' the thermal conductivity, C the solid particles concentration, the total ionic charge density ρ_e, and the gradient of velocity $\boldsymbol{L}$. Ohm's law has the following mathematical form [34]

$$\boldsymbol{J} = \sigma\left(\tilde{\boldsymbol{V}}\times\boldsymbol{B} - \frac{1}{e_0}\left(\tilde{\boldsymbol{V}}\times\boldsymbol{B}\right)\right) \qquad (5)$$

where σ is the fluid's electric conductivity and e_0 is the strength of the electron density. The externally applied electric field, the thermo-electric term, and the polarization impact are assumed to be zero. The Lorentz force with $\boldsymbol{B} = (0, B_0)$ can be examined in the following equation. From Eq. 5, we have [34]

$$\boldsymbol{J}\times\boldsymbol{B} = \frac{-\sigma B_0^2}{m^2+1}\left(\tilde{u}_f - m\tilde{v}_f, m\tilde{u}_f + \tilde{v}_f\right) \qquad (6)$$

where $m = \frac{\sigma B_0}{e_0}$ is the Hall parameter. The Carreau model quantitatively appears as [23–28]:

$$\boldsymbol{\tau}_f = \mu_s\left(1 + (\Gamma\tilde{\gamma})^2\right)^{\frac{n-1}{2}}\tilde{\boldsymbol{\gamma}}. \qquad (7)$$
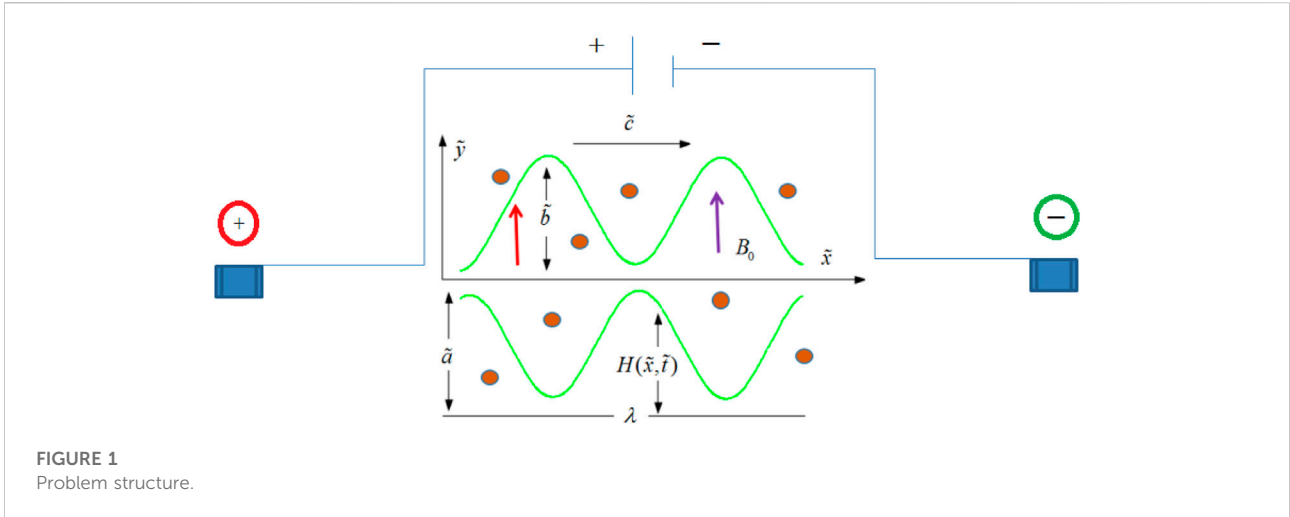
FIGURE 1
Problem structure.

For the particulate phase with velocity $V_p = (\tilde{u}_p, \tilde{v}_p)$, the mathematical model is given as:

$$\boldsymbol{\nabla} \cdot \boldsymbol{V_p} = 0, \tag{8}$$

$$C\rho_p\left(\frac{\partial}{\partial \tilde{t}} + \boldsymbol{V_p} \cdot \boldsymbol{\nabla}\right)\boldsymbol{V_p} = C\boldsymbol{\nabla}\tilde{P} + CS(\boldsymbol{V_p} - \boldsymbol{V_f}), \tag{9}$$

$$C\rho_p c_p\left(\frac{\partial}{\partial \tilde{t}} + \boldsymbol{V_f} \cdot \boldsymbol{\nabla}\right)\tilde{T}_P = \frac{C\rho_p c_p}{\varpi_T}\left(\tilde{T}_P - \tilde{T}_f\right). \tag{10}$$

Electro-osmotic phenomenon

An electric potential is generated due to the presence of EDL on channel surfaces, whose mathematical structure is developed with the following Poisson relation [29–33]:

$$\boldsymbol{\nabla}^2 \bar{\varphi} = -\frac{\rho_e}{\varepsilon}, \tag{11}$$

where ∇^2 represents the Laplace operator, the ionic charge density is $\rho_e = e(n^+ - n^-)z$, $n^\pm$ indicates the strength of oppositely charged ions, ε the permittivity, and e is the single electronic charge. If there is no overlapping, the Boltzmann distribution gives us

$$n^\pm = n_0 \exp\left(\pm \frac{\bar{\varphi}ez}{k_B T}\right). \tag{12}$$

The aforementioned expression contains the bulk concentration of ions as n_0, the charge balance z, the Boltzmann factor k_B, and the average temperature solution k_B. Now, by Debye–Huckel limiting relation, we have

$$\sinh\left(\frac{\bar{\varphi}ez}{k_B T_{av}}\right) \sim \frac{\bar{\varphi}ez}{k_B T_{sol}}. \tag{13}$$

The Boltzman equation is transformed as:

$$\frac{\partial^2 \bar{\varphi}}{\partial \tilde{x}^2} + \frac{\partial^2 \bar{\varphi}}{\partial \tilde{y}^2} = k^2 \bar{\varphi}. \tag{14}$$

Introducing the subsequent non-dimensional quantities

$$\tilde{c}\tilde{t} = \lambda t,\ \tilde{u}_f = \tilde{c}u_f,\ \tilde{v}_f = \delta\tilde{c}v_f,\ \tilde{x} = \lambda x,\ \tilde{y} = \tilde{a}y,\ \tilde{p} = \frac{\lambda\mu_s\tilde{c}}{\tilde{a}^2}p,$$

$$\tilde{\tau} = \frac{\mu_s\tilde{c}}{\tilde{a}^2}\tau, \delta = \frac{\tilde{a}}{\lambda}, \varphi = \frac{\bar{\varphi}}{\varsigma},\ N_1 = \frac{S\tilde{a}^2}{\mu_s},\ M^2 = \frac{\sigma B_0^2 \tilde{a}^2}{\mu_s},$$

$$Re = \frac{\rho_f \tilde{a}\tilde{c}}{\mu_s}, \tilde{\gamma} = \frac{\tilde{c}}{\tilde{a}}\dot{\gamma},\ \tilde{T}_{f,p} = \theta_{f,p}(\tilde{T}_1 - \tilde{T}_0) + \tilde{T}_0,$$

$$P_r = \frac{\mu_s c_p}{k'},\ E_c = \frac{\tilde{c}^2}{c_p(\tilde{T}_1 - T_0)}, U_e = \frac{E_x \varepsilon\varsigma}{\mu c},$$

$$k^2 = \frac{n_0(ez)^2}{\varepsilon k_B T_{sol}} = \left(\frac{\tilde{a}}{\lambda_d}\right)^2. \tag{15}$$

After incorporating aforementioned transformations, Eqs. 2–4, 8–10 become

$$\frac{\partial u_{f,p}}{\partial x} + \frac{\partial u_{f,p}}{\partial y} = 0, \tag{16}$$

$$(1-C)R_e\delta\left(\frac{\partial u_f}{\partial t} + u_f\frac{\partial u_f}{\partial x} + v_f\frac{\partial u_f}{\partial y}\right)$$
$$= -(1-C)\frac{\partial p}{\partial x} + CN_1(u_p - u_f) + (1-C)\left(\delta\frac{\partial}{\partial x}\tau_{xx} + \frac{\partial}{\partial y}\tau_{xy}\right)$$
$$+ \frac{M^2}{(1+m^2)}(m\delta v_f - u_f) + U_e k^2\varphi, \tag{17}$$

$$(1-C)\delta^3 Re\left(\frac{\partial v_f}{\partial t} + u_f\frac{\partial v_f}{\partial x} + v_f\frac{\partial v_f}{\partial y}\right)$$
$$= -(1-C)\frac{\partial p}{\partial y} + \delta(1-C)\left(\delta\frac{\partial \tau_{yx}}{\partial x} + \frac{\partial \tau_{yy}}{\partial y}\right) + \delta^2 CN_1(v_p - v_f)$$
$$- \delta\frac{M^2}{(1+m^2)}(mu_f - \delta v_f) + \delta U_e k^2\varphi, \tag{18}$$

$$Re\left(1-C\right)\delta\left(\frac{\partial\theta_f}{\partial t}+u_f\frac{\partial\theta_f}{\partial x}+v_f\frac{\partial\theta_f}{\partial y}\right)$$

$$=\frac{1}{P_r}\left(1-C\right)\frac{\partial^2\theta_f}{\partial y^2}+CN_1E_c\left(\frac{dp}{dx}\frac{1}{N_1}\right)^2+\left(1-C\right)E_c\tau_{xy}\frac{\partial u_f}{\partial y},$$

$$(19)$$

$$Re\delta\left(\frac{\partial u_p}{\partial t}+u_p\frac{\partial u_p}{\partial x}+v_p\frac{\partial u_p}{\partial y}\right)+\frac{\partial p}{\partial x}=N_1\left(u_f-u_p\right), \quad (20)$$

$$Re\delta^3\left(\frac{\partial v_p}{\partial t}+u_p\frac{\partial v_p}{\partial x}+\delta v_p\frac{\partial v_p}{\partial y}\right)+\frac{\partial p}{\partial y}=\delta^2 N_1\left(v_f-v_p\right). \quad (21)$$

$$\delta\left(\frac{\partial\theta_p}{\partial t}+u_p\frac{\partial\theta_p}{\partial x}+v_p\frac{\partial\theta_p}{\partial y}\right)=\alpha\left(\theta_f-\theta_p\right), \quad (22)$$

where U_e is the Helmholtz–Smoluchowski velocity, ς is zeta potential, and λ_d is Debye length. After defining dimensionless parameters, Eq. 14 becomes

$$\frac{d^2\varphi}{dy^2}=k^2\varphi. \quad (23)$$

with normalized boundary conditions defined as:

$$\frac{\partial\varphi}{\partial y}\bigg|_{y=0}=0 \text{ and } \varphi\big|_{y=h}=0. \quad (24)$$

The potential obtained can be found by solving Eq. 23 along with the boundary conditions given in Eq. 24 as

$$\varphi=\frac{\cosh ky}{\cosh kh}. \quad (25)$$

The square of scalar tensor is measured as:

$$\tilde{\gamma}^2=2\left(\delta\frac{\partial\tilde{u}_f}{\partial\tilde{x}}\right)^2+2\left(\delta\frac{\partial\tilde{v}_f}{\partial\tilde{y}}\right)^2+\left(\frac{\partial\tilde{u}_f}{\partial\tilde{y}}+\delta\frac{\partial\tilde{v}_f}{\partial\tilde{x}}\right)^2, \quad (26)$$

and in their component form, the stress factors are formulated as:

$$\tau_{xx}=2\left(1+\frac{n-1}{2}We^2\tilde{\gamma}^2\right)\delta\frac{\partial u_f}{\partial x},$$

$$\tau_{yy}=2\left(1+\frac{n-1}{2}We^2\tilde{\gamma}^2\right)\delta\frac{\partial v_f}{\partial y},$$

$$\tau_{xy}=\left(1+\frac{n-1}{2}We^2\tilde{\gamma}^2\right)\left(\frac{\partial u_f}{\partial y}+\delta^2\frac{\partial v_f}{\partial x}\right). \quad (27)$$

Considering the lubrication strategy, we finally obtained the following velocity and temperature expressions for dual phases:

$$\frac{1}{1-C}\frac{dp}{dx}=\frac{\partial^2 u_f}{\partial y^2}+\frac{n-1}{2}We^2\frac{\partial^2 u_f}{\partial y^2}\left(\frac{\partial u_f}{\partial y}\right)^2-\frac{1}{1-C}\frac{M^2}{1+m^2}u_f$$

$$+\frac{1}{1-C}U_e k^2\frac{\cosh\left(ky\right)}{\cosh\left(kh\right)}, \quad (28)$$

$$\frac{\partial^2\theta_f}{\partial y^2}+E_c P_r\left[\frac{\partial u_f}{\partial y}+\frac{(n-1)}{2}We^2\left(\frac{\partial u_f}{\partial y}\right)^3\right]\left(\frac{\partial u_f}{\partial y}\right)$$

$$+\frac{CE_c P_r}{N_1\left(1-C\right)}\left(\frac{dp}{dx}\right)^2$$

$$=0, \quad (29)$$

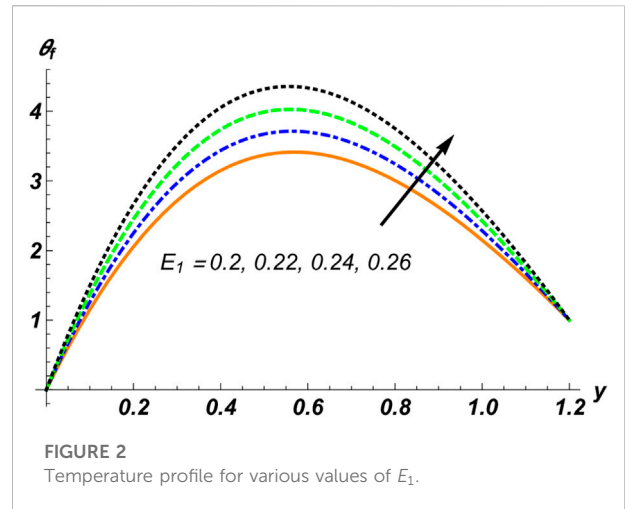$$\frac{dp}{dx}=N_1\left(u_f-u_p\right), \quad (30)$$

FIGURE 2
Temperature profile for various values of E_1.

$$\theta_f=\theta_p. \quad (31)$$

The imposed surface constraints are manufactured as:

$$\frac{\partial\tilde{u}_f}{\partial\tilde{y}}=0, \quad \tilde{T}_f=\tilde{T}_0, \text{ at } \tilde{y}=0, \quad (32)$$

$$\tilde{u}_f=0, \quad \tilde{T}_f=\tilde{T}_1, \quad \text{at} \quad \tilde{y}=H\left(\tilde{x},\tilde{t}\right)=\tilde{a}+\tilde{b}\sin\frac{2\pi}{\lambda}\left(\tilde{x}-\tilde{c}\tilde{t}\right). \quad (33)$$

Their corresponding boundary conditions in dimensionless form are:

$$\frac{\partial u_f}{\partial y}=0, \quad \theta_f=0, \quad \text{at } y=0, \quad (34)$$

$$u_f=0, \quad \theta_f=1, \text{ at } \quad y=h=1+\phi\sin 2\pi\left(x-t\right). \quad (35)$$

The expressions for the particulate viscosity and drag coefficient are reported in [33].

Compliant wall conditions
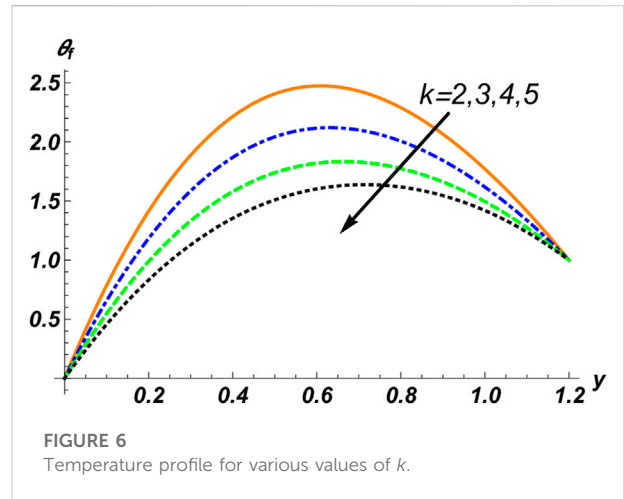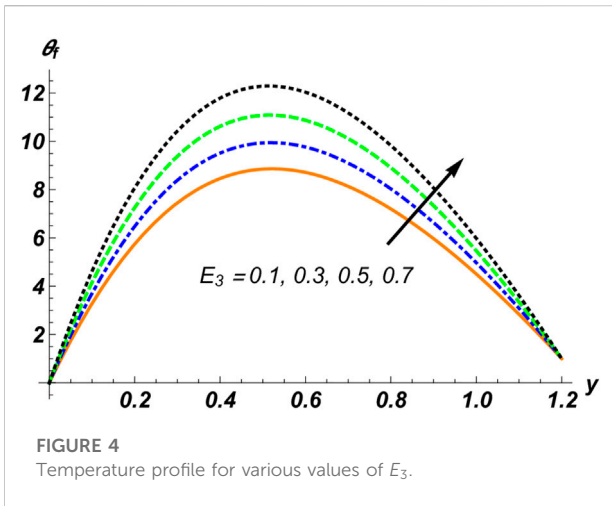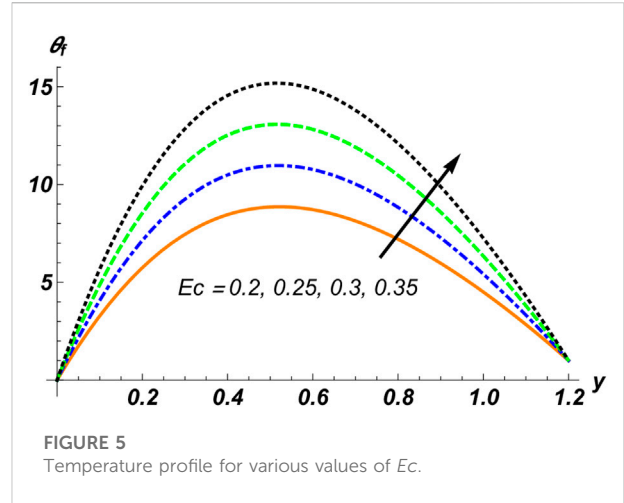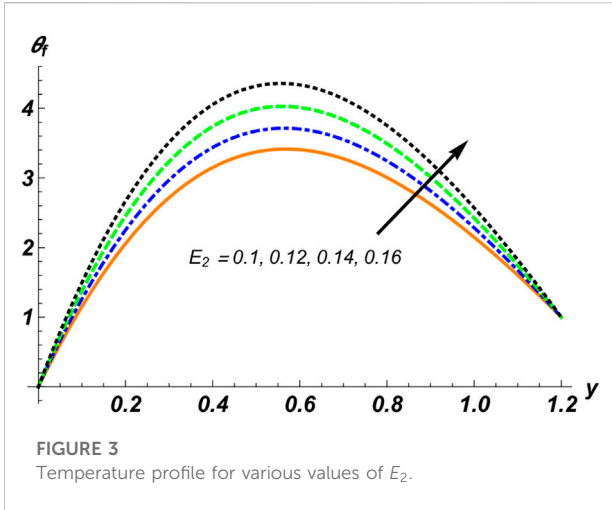
The oscillating boundaries are displayed as [34]:

$$L=p-p_0, \quad (36)$$

where p_0 assumes outside walls' pressure created by muscular tension. A viscosity damping force and a stretched membrane can be represented by the operator described as follows:

$$L=M\frac{\partial^2}{\partial t^2}-T\frac{\partial^2}{\partial x^2}+D\frac{\partial}{\partial t}, \quad (37)$$

$$\frac{\partial p}{\partial x}=E_1\frac{\partial^3\chi}{\partial x^3}+E_2\frac{\partial^3\chi}{\partial t^2\partial x}+E_3\frac{\partial^2\chi}{\partial t\partial x}\,at\,y=1\pm\chi. \quad (38)$$

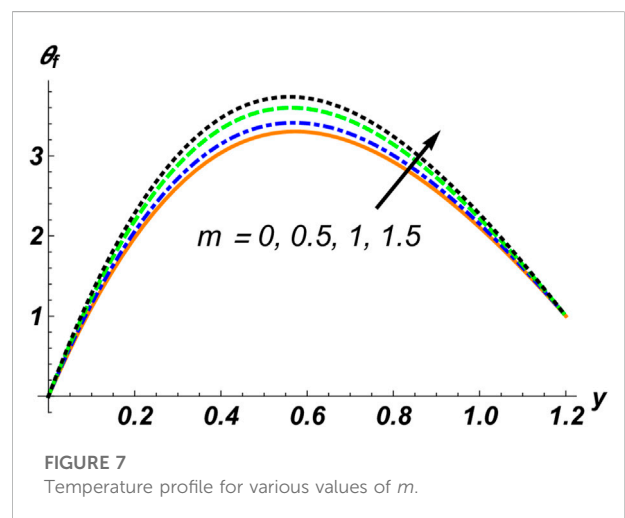In the aforementioned equation, $\chi=\varphi\sin 2\pi\left(x-t\right)$. The dimensionless parameters E_1, E_2, E_3 are defined as:

FIGURE 3
Temperature profile for various values of E_2.

FIGURE 5
Temperature profile for various values of Ec.

FIGURE 4
Temperature profile for various values of E_3.

FIGURE 6
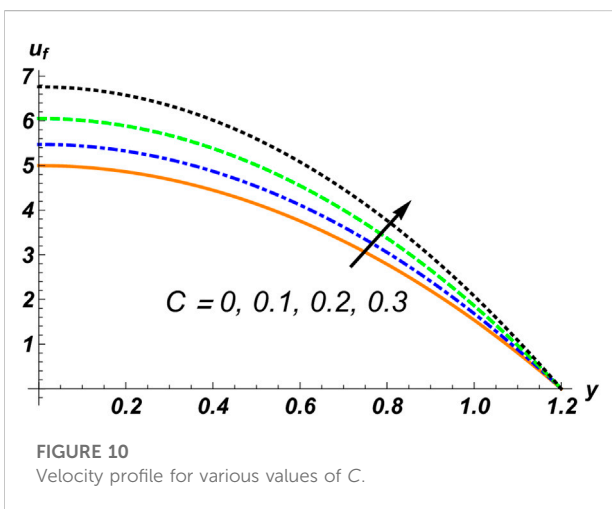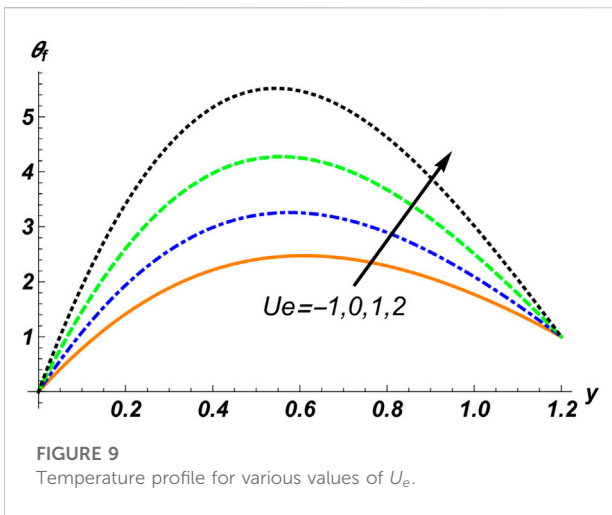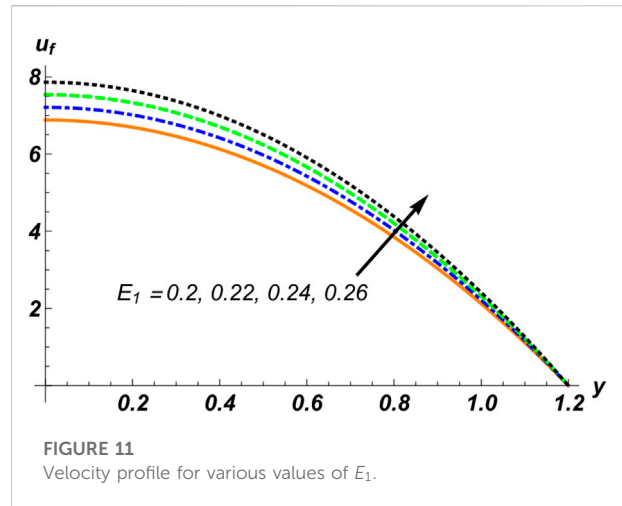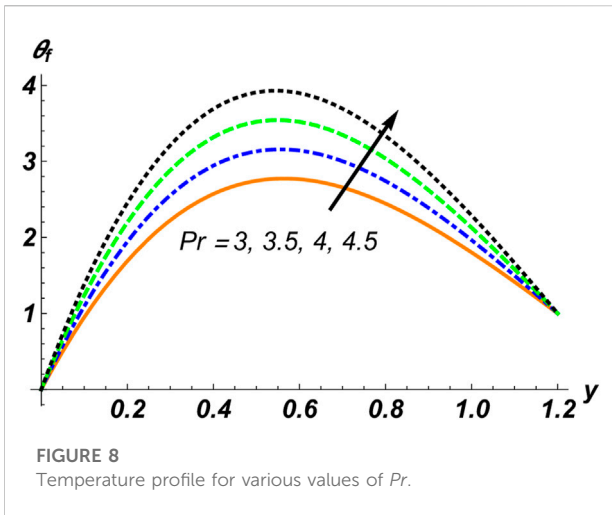Temperature profile for various values of k.

$$E_1 = -\frac{T\tilde{a}^3}{\tilde{c}\lambda^3\mu_s}, \; E_2 = \frac{M\tilde{a}^3\tilde{c}}{\lambda^3\mu_s}, \; E_3 = \frac{D\tilde{a}^3}{\lambda^2\mu_s}. \qquad (39)$$

Numerical results and discussion

Eqs. 28, 29 are nonlinear coupled differential equations whose exact solution is a very difficult task, so a numerical solution for the considered problem was developed using the computational software Mathematica with the built-in NDSolve tool. The data obtained numerically have been plotted for various physical factors. Here, we discuss the results of various considerable profiles of the problem graphically by sketching plots against some key parameters of the study while keeping others fixed. For this, graphs of temperature profile θ_f are placed

FIGURE 7
Temperature profile for various values of m.

FIGURE 8
Temperature profile for various values of Pr.

FIGURE 11
Velocity profile for various values of E_1.

FIGURE 9
Temperature profile for various values of U_e.

FIGURE 10
Velocity profile for various values of C.

in Figures 2–9 while the velocity variation of the fluid is presented in Figures 10–14.

Figures 2–4 are manipulated for the parameters E_1, E_2 and E_3 respectively. It is quite visible in these diagrams that temperature is an increasing function of the aforementioned factors, but it is also quite noticeable that while there is a significant variation in temperature, with small changes in the values of E_1 and E_2, for E_3, we require a large difference in parametric values. Thus, the elastic property of the walls can help increase the speed of the thermal exchange process. Moreover, the damping force of the walls can exert much impact on the transfer of heat from the lower to the upper surface due to a decrease in oscillation of the compliant walls. This damping can be produced due to energy dissipation due to the oscillation of the walls so in return, the total amount of heat exchange increases. If we consider Figure 5, which is plotted for Eckert number E_c, we can identify a direct relation between θ_f and E_c. This means that an increase in wave speed by keeping the specific heat of the fluid uniform and by maintaining the temperature balance of the flow region can enlarge the procedure of heat exchange. The electro-kinetic parameter k is included in Figure 6 to investigate the influence on heat distribution, and we can see that when we increase its value, the temperature θ_f falls. It is also quite interesting to note that for an initial change in the values of the parameter, there is a large variation in the curves, but for further increases, the variation becomes minute. It can be taken from this observation that the kinetic energy induced due to the electric field provided by the external battery voltage can function as resistance to vary the temperature of the medium, such that a small quantity of heat will be transferred from the lower wall to the upper one in case of a larger contribution of kinetic energy. From Figure 7, we can guess the effects of two parameter Hall current factor m. This plot suggests that there is an increase in temperature distribution with m. Figures 8 and 9 show the variation in thermal exchange along the Prandtl number Pr

FIGURE 12
Velocity profile for various values of E_2.

FIGURE 15
Velocity profile for various values of Ue.

FIGURE 13
Velocity profile for various values of k.

FIGURE 14
Velocity profile for various values of m.
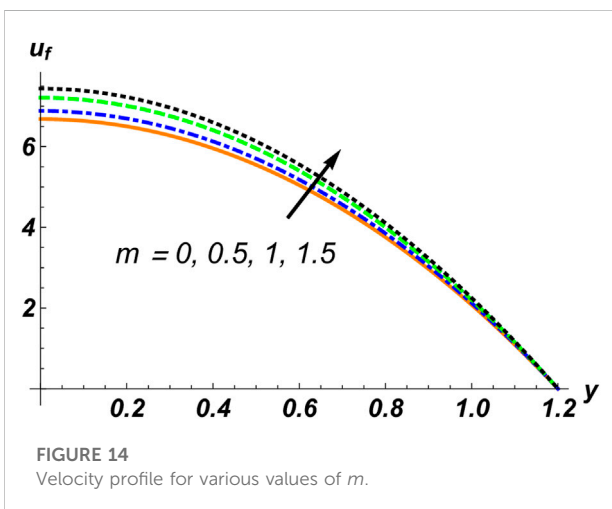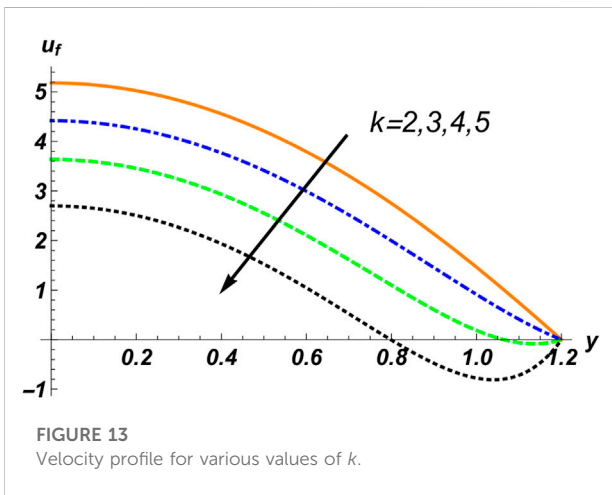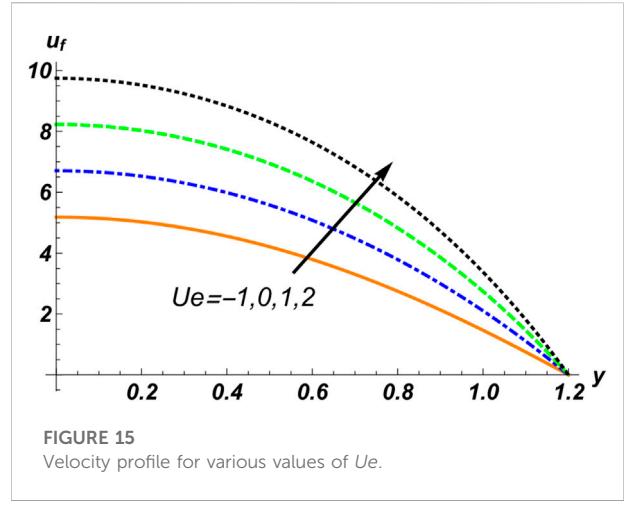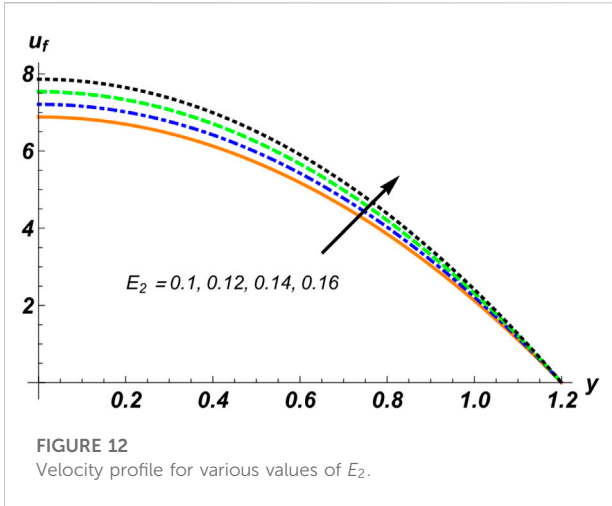
and Helmholtz–Smoluchowski velocity Ue, accordingly. From these images, it can be inferred that temperature distribution increases due to incremental changes in Pr and Ue. A large Prandtl number may be due to the increasing momentum diffusivity and by keeping the thermal diffusivity fixed or by decreasing the thermal diffusivity and keeping the momentum diffusivity constant. This means that if we increase the momentum diffusivity of the Carreau fluid, the thermal profile increases, which may be due to entropy production in the system due to the variable viscosity of the fluid.

Velocity graphs are shown in Figures 10–15. Figure 10 presents the solid particle concentration C, which affects the velocity of the fluid in an increasing manner, such that if we increase the concentration of solid particles, the velocity of the fluid increases. The kind of observation can be obtained in Figures 11 and 12, which indicate the reflection of the compliant wall parameters E_1 and E_2, respectively, on the fluid phase axial velocity function u_f. It is notable that all factors increase the velocity of the streams. This is due to the physical fact that with a large damping force, the oscillations of the compliant walls are reduced, which results in a smoothing of the flow particles and an enhanced speed of the liquid. Moreover, the elasticity of the walls also helps push the fluid molecules much faster than the normal flow. From Figure 13, it seems clear that the velocity slows as we raise the magnitude of the electro kinetic factor k, and the reverse flow is also measurable on the right side of the channel. It is suggested that kinetic energy appears as an external force that exerts extra pressure on the flow molecules, and in return, the flow speed becomes untidy. Figure 14 indicates that a fluid's speed is enhanced in the case of an increase in the Hall current m. Figure 15 shows the variation in velocity distribution u_f for Helmholtz–Smoluchowski velocity Ue. Thus, Ue has a direct impact on velocity.

Conclusion

A numerical investigation is conducted to analyze the theoretical study of peristaltic flow of a Carreau fluid model in a channel with thermally induced compliant walls in the presence of electro-osmosis and Hall current effects. To estimate the effects of different valuable factors of the flow problem, graphs have been sketched that show the monotonic variation of temperature and velocity profiles. From the graphical presentation, we draw some key findings, listed as follows:

1. Temperature distribution increases with the concentration of solid particles, the rigidity of the walls, the Hall current factor, the Helmholtz–Smoluchowski velocity, and the Prandtl number.
2. The magnetic field, the electro-kinetic parameter, and the Weissenberg number have an inverse relationship with thermal exchange.
3. The velocity of the fluid phase is directly proportional to the distribution of solid particles, the compliant wall factor, the Hall current parameter, and the Helmholtz–Smoluchowski velocity.
4. The magnetic field, the electro-kinetic parameter, and the Weissenberg number are in inverse relation to the fluid's velocity.
5. Future work can be performed on this problem by inserting heat and mass transfer effects and elaborating the entropy generation in the flow.
6. It is also notable that this study can be validated in relation to the previous relevant literature by neglecting the electro-osmotic effects. Moreover previous study on the topic [30] can be evaluated with a numerical technique of parallel shooting, and the current data are collected using the built-in Mathematica tool NDSolve to produce a more authentic numerical reading.
7. In future, we can discuss entropy generation and mass transfer effects to obtain new results.

Data availability statement

The original contributions presented in the study are included in the article/Supplementary Material, and further inquiries can be directed to the corresponding author.

Author contributions

All authors listed have made a substantial, direct, and intellectual contribution to the work and approved it for publication.

Acknowledgments

Conflict of interest

The authors declare that the research was conducted in the absence of any commercial or financial relationships that could be construed as a potential conflict of interest.

Publisher's note

All claims expressed in this article are solely those of the authors and do not necessarily represent those of their affiliated organizations, or those of the publisher, the editors, and the reviewers. Any product that may be evaluated in this article, or claim that may be made by its manufacturer, is not guaranteed or endorsed by the publisher.

References

1. Latham TW. *Fluid motions in a peristaltic pump*. Doctoral dissertation, Massachusetts Institute of Technology (1966).

2. Fung YC, Yih CS. *Peristaltic transport* (1968).

3. Shapiro AH, Jaffrin MY, Weinberg SL. Peristaltic pumping with long wavelengths at low Reynolds number. *J Fluid Mech* (1969) 37(4):799–825. doi:10.1017/s0022112069000899

4. Salahuddin T, Khan I, Malik MY, Khan M, Hussain A, Awais M. Internal friction between fluid particles of MHD tangent hyperbolic fluid with heat generation: Using coefficients improved by Cash and Karp. *Eur Phys J Plus* (2017) 132(5):205–10. doi:10.1140/epjp/i2017-11477-9

5. Sridhar V, Ramesh K, Gnaneswara Reddy M, Azese MN, Abdelsalam SI. On the entropy optimization of hemodynamic peristaltic pumping of a nanofluid with geometry effects. In: *Waves in random and complex media* (2022). p. 1–21.

6. Abdelsalam SI, Mekheimer KS, Zaher AZ. Dynamism of a hybrid Casson nanofluid with laser radiation and chemical reaction through sinusoidal channels. *Waves in Random and Complex Media* (2022) 1–22. doi:10.1080/17455030.2022.2058714

7. Khan M, Salahuddin T, Malik MY, Khan F. Arrhenius activation in MHD radiative Maxwell nanoliquid flow along with transformed internal energy. *Eur Phys J Plus* (2019) 134(5):198. doi:10.1140/epjp/i2019-12563-8

8. Khan M, Salahuddin T, Malik MY. Implementation of Darcy–forchheimer effect on magnetohydrodynamic carreau–yasuda nanofluid flow: Application of von kármán. *Can J Phys* (2019) 97(6): 670–7. doi:10.1139/cjp-2018-0547

9. Bhatti MM, Zeeshan A. Study of variable magnetic field and endoscope on peristaltic blood flow of particle-fluid suspension through an annulus. *Biomed Eng Lett* (2016) 6(4):242–9. doi:10.1007/s13534-016-0226-2

10. Bhatti MM, Zeeshan A, Ellahi R. Study of heat transfer with nonlinear thermal radiation on sinusoidal motion of magnetic solid particles in a dusty fluid. *J Theor Appl Mech* (2016) 46(3):75–94. doi:10.1515/jtam-2016-0017

11. Bhatti MM, Zeeshan A, Ijaz N. Slip effects and endoscopy analysis on blood flow of particle-fluid suspension induced by peristaltic wave. *J Mol Liquids* (2016) 218:240–5. doi:10.1016/j.molliq.2016.02.066

12. Srivastava LM, Srivastava VP. Peristaltic transport of blood: Casson model—II. *J Biomech* (1984) 17(11):821–9. doi:10.1016/0021-9290(84)90140-4

13. Srivastava LM, Srivastava VP. *Peristaltic transport of a particle-fluid suspension* (1989).

14. Misra JC, Pandey SK. Peristaltic transport of a particle-fluid suspension in a cylindrical tube. *Comput Math Appl* (1994) 28(4):131–45. doi:10.1016/0898-1221(94)00134-0

15. Yamane K, Nakagawa M, Altobelli SA, Tanaka T, Tsuji Y. Steady particulate flows in a horizontal rotating cylinder. *Phys Fluids* (1998) 10(6):1419–27. doi:10.1063/1.869858

16. Bhatti MM, Zeeshan A, Ellahi R. Heat transfer analysis on peristaltically induced motion of particle-fluid suspension with variable viscosity: Clot blood model. *Comp Methods Programs Biomed* (2016) 137:115–24. doi:10.1016/j.cmpb.2016.09.010

17. Akram J, Akbar NS, Maraj E. Chemical reaction and heat source/sink effect on magnetonano Prandtl-Eyring fluid peristaltic propulsion in an inclined symmetric channel. *Chin J Phys* (2020) 65:300–13. doi:10.1016/j.cjph.2020.03.004

18. Rashed ZZ, Ahmed SE. Peristaltic flow of dusty nanofluids in curved channels. *Comput Mater Continua* (2021) 66(1):1012–26. doi:10.32604/cmc.2020.012468

19. Akbar NS, Maraj EN, Noor NFM, Habib MB. Exact solutions of an unsteady thermal conductive pressure driven peristaltic transport with temperature-dependent nanofluid viscosity. *Case Stud Therm Eng* (2022) 35:102124. doi:10.1016/j.csite.2022.102124

20. Nazeer M, Al-Zubaidi A, Hussain F, Duraihem FZ, Anila S, Saleem S. Thermal transport of two-phase physiological flow of non-Newtonian fluid through an inclined channel with flexible walls. *Case Stud Therm Eng* (2022) 35:102146. doi:10.1016/j.csite.2022.102146

21. Saleem S, Subia GS, Nazeer M, Hussain F, Hameed MK. Theoretical study of electro-osmotic multiphase flow of Jeffrey fluid in a divergent channel with lubricated walls. *Int Commun Heat Mass Transfer* (2021) 127:105548. doi:10.1016/j.icheatmasstransfer.2021.105548

22. Riaz A, Sadiq MA. Particle–fluid suspension of a non-Newtonian fluid through a curved passage: An application of urinary tract infections. *Front Phys* (2020) 8:109. doi:10.3389/fphy.2020.00109

23. Noreen S, Kausar T, Tripathi D, Ain QU, Lu DC. Heat transfer analysis on creeping flow Carreau fluid driven by peristaltic pumping in an inclined asymmetric channel. *Therm Sci Eng Prog* (2020) 17:100486. doi:10.1016/j.tsep.2020.100486

24. Asha SK, Beleri J. Peristaltic flow of Carreau nanofluid in presence of Joule heat effect in an inclined asymmetric channel by multi-step differential transformation method. *World Scientific News* (2022) 164:44–63.

25. Maqbool K, Manzoor N, Ellahi R, Sait SM. Influence of heat transfer on MHD Carreau fluid flow due to motile cilia in a channel. *J Therm Anal Calorim* (2021) 144(6):2317–26. doi:10.1007/s10973-020-10476-6

26. Vajravelu K, Sreenadh S, Saravana R. Combined influence of velocity slip, temperature and concentration jump conditions on MHD peristaltic transport of a Carreau fluid in a non-uniform channel. *Appl Math Comput* (2013) 225:656–76. doi:10.1016/j.amc.2013.10.014

27. Alsemiry RD, Sayed HM, Amin N. Mathematical analysis of Carreau fluid flow and heat transfer within an eccentric catheterized artery. *Alexandria Eng J* (2022) 61(1):523–39. doi:10.1016/j.aej.2021.06.029

28. Bilal Ashraf M, Haq SU. The convective flow of Carreau fluid over a curved stretching surface with homogeneous-heterogeneous reactions and viscous dissipation. *Waves in Random and Complex Media* (2022) 1–15. doi:10.1080/17455030.2022.2032867

29. Yasmin H, Iqbal N. Convective mass/heat analysis of an electroosmotic peristaltic flow of ionic liquid in a symmetric porous microchannel with soret and dufour. *Math Probl Eng* (2021) 1–14. doi:10.1155/2021/2638647

30. Tripathi D, Bhushan S, Bég OA. Unsteady viscous flow driven by the combined effects of peristalsis and electro-osmosis. *Alexandria Eng J* (2018) 57(3):1349–59. doi:10.1016/j.aej.2017.05.027

31. Prakash J, Tripathi D. Study of EDL phenomenon in Peristaltic pumping of a Phan-Thien-Tanner Fluid through asymmetric channel. *Korea-aust Rheol J* (2020) 32(4):271–85. doi:10.1007/s13367-020-0026-1

32. Akram J, Akbar NS, Tripathi D. Analysis of electroosmotic flow of silver-water nanofluid regulated by peristalsis using two different approaches for nanofluid. *J Comput Sci* (2022) 62:101696. doi:10.1016/j.jocs.2022.101696

33. Akram J, Akbar NS, Tripathi D. Entropy generation in electroosmotically aided peristaltic pumping of MoS2 Rabinowitsch nanofluid. *Fluid Dyn Res* (2022) 54(1):015507. doi:10.1088/1873-7005/ac4e7b

34. Alsharif AM, Abdellateef AI, Elmaboud YA, Abdelsalam SI. Performance enhancement of a DC-operated micropump with electroosmosis in a hybrid nanofluid: Fractional cattaneo heat flux problem. *Appl Math Mech* (2022) 43(6):931–44. doi:10.1007/s10483-022-2854-6

35. Bhatti MM, Ellahi R, Zeeshan A, Marin M, Ijaz N. Numerical study of heat transfer and Hall current impact on peristaltic propulsion of particle-fluid suspension with compliant wall properties. *Mod Phys Lett B* (2019) 33(35):1950439. doi:10.1142/s0217984919504396